Journal of the Serbian Chemical Society
JSCS@tmf.bg.ac.rs • www.shd.org.rs/JSCS
J. Serb. Chem. Soc. 88 (12) 1355–1367 (2023)
JSCS–5700
Original scientific paper
Published 19 December 2023

Zn(II) complex with pyridine based 1,3-selenazolyl-hydrazone: Synthesis, structural characterization and DFT study

JOVANA B. ARAŠKOV[1#], PREDRAG G. RISTIĆ[1*#], ALEKSANDAR VIŠNJEVAC[2**], ANDREJ LJ. MILIVOJAC[3], DRAGANA M. MITIĆ[3], NENAD R. FILIPOVIĆ[4#] and TAMARA R. TODOROVIĆ[1#]

[1]University of Belgrade – Faculty of Chemistry, Studentski trg 12–16, 11000 Belgrade, Serbia, [2]Division of Physical Chemistry, Institute Ruđer Bošković, Bijenička cesta 54, Zagreb 10000, Croatia, [3]Innovation Centre of Faculty of Chemistry, University of Belgrade, Studentski trg 12–16, 11000 Belgrade, Serbia and [4]University of Belgrade – Faculty of Agriculture, Nemanjina 6, 11000 Belgrade, Serbia

(Received 31 August, revised 25 September, accepted 13 October 2023)

Abstract: An octahedral complex of Zn(II) with a ligand from a class of pyridine-based 1,3-selenazolyl-hydrazones was synthesized and characterized by IR and NMR spectroscopy and single crystal X-ray diffraction analysis. The purity of the complex was confirmed by elemental analysis. Two ligands are coordinated in the neutral *NNN*-tridentate form forming a complex cation, while the positive charge is neutralized by $[ZnCl_4]^{2-}$. Complex crystallizes in monoclinic *C*2/*c* space group with the Zn atoms situated in a special position. The packing features of the novel complex were analyzed using Hirshfeld surfaces, construction of 2D pseudosymmetric plot and DFT quantum mechanical calculations and compared with the previously published sulfur-based isostere. The key difference in the structures, imposed by replacement of sulfur with selenium, were identified.

Keywords: Zn(II) complex; selenazolyl-hydrazones; X-ray crystal structure; isosteres; selenium; intermolecular energies.

INTRODUCTION

Zinc is one of the most studied elements in pharmacological research due to the fact that it is found in about 10 % of all enzymes in human body. Also, zinc is a versatile element extensively employed in various area of material chemistry research, including nanomaterial synthesis,[1,2] photocatalytic,[3] photoluminescence[4,5] and electrochemical[6] studies. The possibility of achieving different coordination numbers from 2 to 9 (most often 4-6)[7], affinity to *N*,*O*,*S*-donor

* Corresponding authors. E-mail: (*)predrag@chem.bg.ac.rs, (**)visnevac@irb.hr
# Serbian Chemical Society member.
https://doi.org/10.2298/JSC230831079A

atoms and high bioavailability makes Zn(II) an excellent candidate for the synthesis of complexes for specific application. By choosing the starting Zn(II) salt it is possible to control the nuclearity, geometry and type of complexes.

A crystallographic study of complexes provides insight into the geometrical parameters, the orientation of the hydrophilic/phobic parts of the ligands, as well as the types and distribution of weak intermolecular interactions which are important for examining potential application.[8,9]

N-heteroaromatic (1,3-thiazolyl-2-yl)-hydrazones are a widely studied class of compounds as a potential anticancer,[10,11] antioxidant,[12–18] antibacterial,[19–22] antifungal[23–28] and antiparazitic agents.[29,30] By suitable selection of *N*-heteroaromatic moiety and substituents on 1,3-thiazole ring, it is possible to design and direct the coordination mode. An isosteric replacement of sulfur with selenium can lead not only to increase of structural diversity, but also to improvement of pharmacological properties and achievement of a better intake of selenium.[31]

Selenium is a micronutrient that supports the processes of the immune response, fertility, proper function of thyroid hormones, regulation of redox balance in cells and cancer chemoprevention.[32] Also, there are several studies that explain the fact that selenium as a part of organic molecule is more acceptable to the human body than selenium in an inorganic form (such as SeO_3^{2-}).[32,33] In support of the growing field of research on 1,3-selenazole derivatives is the fact that there are 69 crystal structures deposited in CSD[7] containing substituted 1,3-selenazole ring. Two of 69 crystal structures containing the hydrazone pharmacophore as a substituent in 2-position of 1,3-selenazole ring. Eight of the 69 crystal structures are complexes of Zn(II), Co(III) and Cd(II) with *N*-heteroaromatic (1,3-selenazolyl-2-yl)-hydrazones. Since the properties of a complex is dependent not only on the nature of the ligand, but also on weak interactions, this paper presents a crystallographic study and analysis of intermolecular interactions in the crystal structure of novel Zn(II) complex with 2-(2-(pyridine-2-ylmethylene)hydrazonyl)-4--(4-methoxyphenyl)-1,3-selenazole ($HLSe^2$) and comparison with a previously published sulfur isostere.[4]

EXPERIMENTAL

Materials and methods

Potassium selenocyanate (99 %), hydrazine hydrate (99 %), 2-formylpyridine (99 %) and 2-4'-methoxyacetophenone (98 %) were obtained from Acros Organics. Anhydrous $ZnCl_2$ (99 %) was obtained from Merck. All solvents were obtained from commercial suppliers and used without further purification. Purity of complex was confirmed by elemental analysis (C, H, N) by the standard micromethods using the Elementar Vario EL III CHNS/O analyzer. Infra-red (IR) spectra were recorded on a Thermo Scientific Nicolet Summit FT-IR spectrometer by the attenuated total reflection (ATR) technique in the region 4000–400 cm^{-1}. Molar conductivities were measured at room temperature (298 K) on the Crison multimeter MM41. The NMR spectra were performed on a Varian/Aglient 400 MHz. Chemical shifts are given on δ scale relative to tetramethylsilane (TMS) as internal standard for ^1H and ^{13}C. IR and NMR spectra,

as well as analytical and spectral data, are given in Figs. S-1–S-3 of the Supplementary material to this paper.

Synthesis

The ligand based on (1,3-selenazol-2-yl)hydrazone was synthesized according to a previously published procedure.[34] The ligand (50 mg, 0.14 mmol) was dissolved in 10 ml of hot MeOH. When the ligand was dissolved, the solid $ZnCl_2$ (19 mg, 0.14 mmol) was added. The dark orange solution was refluxed for 1 h. After 2 days, orange single crystals of the complex suitable for single crystal X-ray diffraction analysis crystallized from the mother liquor. The crystals were collected by filtration, washed with cold methanol (4 °C) and diethyl ether and dried in a desiccator. Yield: 0.057 g (83 %).

X-ray structural analysis (XRD)

The **2-Cl-Se** (Zn(II) complex with 2-(2-(pyridin-2-ylmethylene)hydrazonyl)-4-(4-methoxyphenyl)-1,3-selenazole) was obtained as single crystal, so its structure in solid state was solved by single crystal X-ray diffraction analysis. Diffraction data for **2-Cl-Se** were collected at 298 K at Xcalibur Ruby Nova diffractometer using monochromatic CuKα (λ = 1.54184 Å) radiation. Collection, data reduction and unit cell refinement was performed using CrysAlisPro.[35] Structure refinement was performed using SHELXL-2016/4.[36] Collected data were corrected for absorption effects using multiple scan absorption correction method. Most of the hydrogen atoms are placed in ideal geometric positions while some are found in the differential Fourier map. Calculations for verification of molecular structures, parameters of crystal packing as well as preparation of illustrations of molecular structures and crystal packing were performed using Platon,[37] Mercury.[38] WinGX[39] and OLEX2[40] programs. Crystallographic information file is deposited in CSD under the following number – 2291805. Crystal data and structure refinement are given in Table S-I of the Supplementary material. Tables of bond angles and lengths are given in Supplementary material (Tables S-II and S-III).

Hirshfeld surfaces and analysis of intermolecular interactions

Hirschfeld surfaces and pseudosymmetric fingerprint plots of intermolecular interactions were generated using crystallographic information file (CIF). Before calculation, bond lengths involving hydrogen atoms were normalized to standard values estimated by neutron diffraction. Visualization of surfaces and presentation of results as d_{norm}, shape indexes and curvedness, as well as calculations of 2D plots with d_e and d_i distance values were done using CrystalExplorer 21[41]. The distance from the surface to the nearest nucleus of the atom on the outside of the surface is denoted as *de*, while the distance from the surface to the closest nucleus of the atom on the inside of the surface is denoted as *di*. The surfaces are mapped over a standard color scale, and 2D fingerprint plots are calculated using *de* and *di* values in the range 0.4−2.8 Å.

Calculation of intermolecular interaction energies

Intermolecular interaction energies were calculated using molecular electron densities derived from wavefunctions computed by Gaussian09[42] coupled with CrystalExplorer21[41] using B3LYP functional[43–46] and DGDZVP basis set.[47,48] CIF is used as input file while bond lengths involving hydrogen atoms were normalized to standard values estimated by neutron diffraction. For calculation purposes, a cluster is constructed around the central molecule which implies real molecular environments and usage of corresponding atomic coordinates at a distance of 3.8 Å from the central molecule. Calculated wave functions were automatically

generated for all symmetrically connected molecules within the cluster and Energy frameworks[49] were constructed for the supercell (2×2×2).

RESULTS AND DISCUSSION

Synthesis and spectroscopic characterization

The complex was synthesized by direct reaction between anhydrous $ZnCl_2$ and $HLSe^2$ (in equimolar ratio) in methanol under reflux conditions (Scheme 1). Based on the results of elemental analysis and molar conductivity measurements, the following molecular formula of the complex was determined: $[Zn(HLSe^2)_2][ZnCl_4]$. The presence of the valence C=N vibration of thiazole ring and the imine bond in IR spectrum was observed at 1564 and 1526 cm^{-1}, respectively. These bands are shifted in the spectrum of **2-Cl-Se** at 1610 and 1546 cm^{-1}, respectively, which indicates coordination of the ligands *via* thiazole and imine nitrogens. Band at 3099 cm^{-1} originates from valence N–H vibration which implies that the ligands are coordinated in a neutral form. In ^{1}H-NMR spectrum presence of N–H at 12.46 ppm additionally confirms coordination of ligands in neutral form. Aromatic protons are in range 6.93–8.54 ppm. At 3.75 ppm singlet originating from the proton of the methoxy group on the periphery of the ligand was observed.

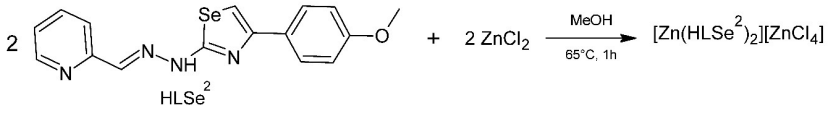

Scheme 1. Synthesis of **2-Cl-Se**.

Molecular structure analysis

Complex **2-Cl-Se** crystallize in the monoclinic *C*2/*c* space group. The complex cation consists of Zn(II) atom and two meridionally positioned ligands coordinated in a neutral form, where the positive charge of the complex cation is neutralized by the tetrachloridozincate(II) anion. (Fig. 1). The geometry of the coordination environment is distorted octahedral where each ligand forms the NNN-chelate tridentate coordination *via* pyridine, imine and azomethine nitrogen atoms. The angular distortion from the ideal octahedron geometry is caused by the position of nitrogen atoms and planarity of the ligand. The Zn atoms are in a special position (Wyckoff letter *e*, site symmetry 2) which causes that the asymmetric unit consists of one half of the complex cation and one half of the tetrachloridozincate(II) anion.

In order to visually describe the geometrical differences in the molecular geometry between the isostructural **2-Cl** (Zn(II) complex with 2-(2-(pyridin-2-ylmethylene)hydrazonyl)-4-(4-methoxyphenyl)-1,3-thiazole) and **2-Cl-Se**, the cations were overlapped over the donor atoms and the deviations from the root

mean planes through the aromatic rings were measured. The substitution of sulfur by selenium atom leads to slight deviations: the mean planes drawn through the rings **A** and **A'** deviate by 3.90°, **B** and **B'** by 2.39°, while the corresponding angle between **C** and **C'** is 2.89° (Fig. 2). The measured deviations are in accordance with the size of sulfur and selenium atoms.

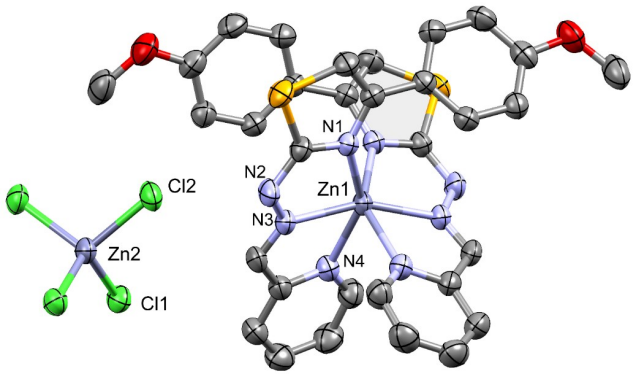

Fig. 1. ORTEP[38] drawing of complex **2-Cl-Se**. Displacement ellipsoids are given in 50 % probability level. Hydrogen atoms are omitted for clarity.

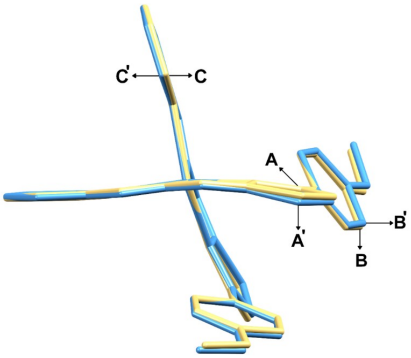

Fig. 2. Overlay of the complex cations of **2-Cl-Se** (yellow) and **2-Cl** (blue). Notation of aromatic rings: 1,3-thiazole/selenazole (**A/A'**), methoxyphenyl (**B/B'**) and pyridine (**C/C'**).

Crystal structure and Hirshfeld surface analysis

A comparative study of intermolecular interactions in isostructural **2-Cl** and **2-Cl-Se** by combined crystal packing and Hirshfeld surface analysis provides valuable insight into key structural differences between them. The contributions of intermolecular interactions in **2-Cl-Se** are represented in the 2D pseudosymmetric plot by red circles (Fig. 3) and quantified and compared to the sulfur isostere in Table I. The analysis of surface area included in intermolecular interactions shows that both crystal packings are based predominantly on classical and non-classical hydrogen interactions which account for 52.8 (**2-Cl-Se**) and

52.9 % (**2-Cl**) of all interactions. The orientations of adjacent cations and anions are in such a position that π–π stacking and anion–π interactions occur (8.5 in **2-Cl-Se** and 7.9 % in **2-Cl**). Hydrophobic interactions are slightly represented in **2-Cl-Se**, which is a consequence of the isosteric replacement of sulfur by selenium atom and is caused by the higher polarizability of selenium atom. The remaining contacts in the case of both complexes are H–H contacts.

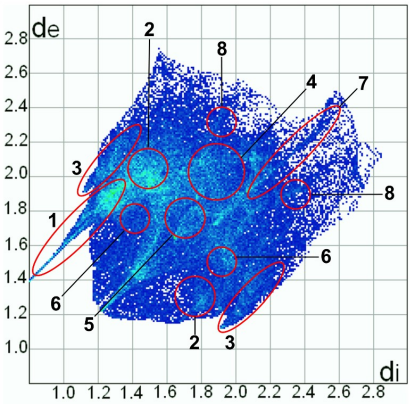

Fig. 3. 2D pseudosymmetric plot of intermolecular interactions in **2-Cl-Se**. Numbered regions correspond to contacts shown in Table I.

TABLE I. Relative contribution of the Hirshfeld surface to individual intermolecular interactions (H···H contacts are disregarded) in the crystal structure of **2-Cl-Se** and **2-Cl**

Complex	Label of interaction							
	1	2	3	4	5	6	7	8
	Interaction type							
	H···Cl	H···C	H···Se(S)	H···O	C···C	H···N	Se(S)···Cl	C···O
2-Cl-Se	19.0	18.1	9.7	4.9	3.6	1.1	2.2	2.7
2-Cl[4]	18.8	18.8	9.3	5.2	3.4	0.8	1.7	2.8

On the Hirshfeld surface most common H···Cl interactions are observed as red patches (Fig. 4A). The complex cation is a double donor in classical (N2––H2A···Cl2, d = 2.287 Å, i = 1–x, y, 1/2–z) and non-classical (C11–H11···Cl1^{i}, d = 2.744 Å; i = 1–x, y, 1/2–z) hydrogen interactions with the tetrachloridezincate(II) anion, which results in the formation of a 1D chain parallel to the *a*-crystallographic axis (Fig. 4B). A higher level of assembly is based on the linking of 1D chains by interactions marked with orange circles on Hirshfeld surface (Fig. 4C). By non-classical C14–H14···Cl2^{ii} interactions (d = 2.932 Å; ii = 1/2–x, 1.5–y, 1–z), the chains are connected in a 2D "pleated" layer parallel to the *ac*-crystallographic plane (Fig. 4D). The remaining interactions are responsible for stacking of 2D layers into the final 3D crystal structure (Fig. 4E). Hydrophobic C–H···π and π···π stacking interactions with a total contribution of 21.7 %

participate of the existence of 3D packing through C10–H10B··· $\pi_{pyridin}$ ^{iii} (d = = 3.956 Å; *iii* = x, 1–y, 1/2+z) and $\pi_{methoxyphenyl}$···$\pi_{pyridine}$^{iv} (d = 3.461 Å; *iv* = = –1/2–x, –1/2+y, 1/2–z).

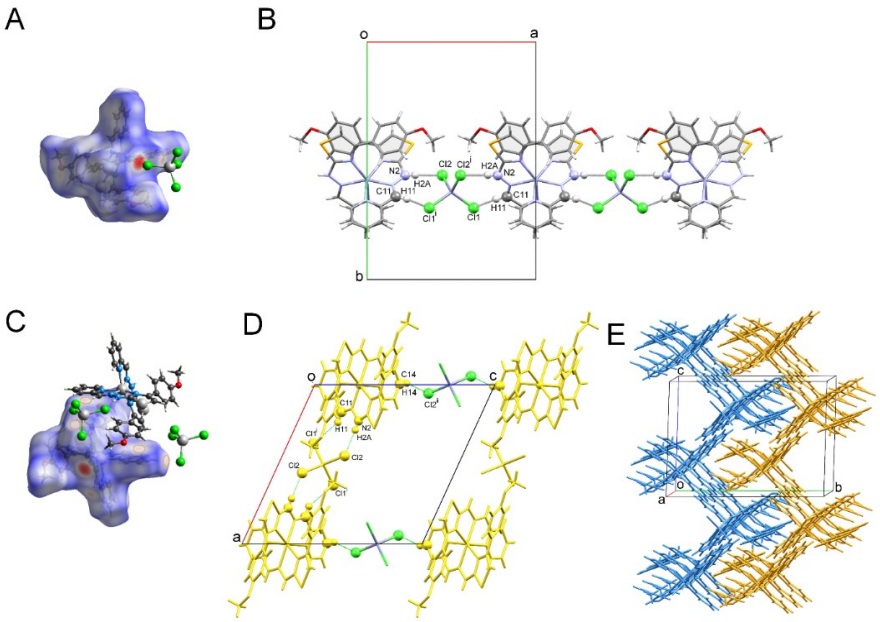

Fig. 4. Hirshfeld d_{norm} surface for **2-Cl-Se** with neighboring tetrachloridozincate(II) anion responsible for formation of 1D chain (A); 1D chain formed parallel to the *a*-crystallographic axis (B); Hirshfeld d_{norm} surface with neighboring species responsible for the formation of 2D and 3D crystal packing (C); Part of a 2D "pleated" layer formed due to the connection of 1D chains (yellow, D). The resulting 3D crystal packing as a result of stacking 2D layers (blue and ochre, E).

Analysis of intermolecular interactions by generating full interaction maps (FIM) using Mercury[38] also provides insight into geometrical analysis of intermolecular interactions grouping them into (non)classical and hydrophobic (aromatic) interactions. Fig. 5A shows a 3D map of the highest probability of finding interactions between certain functional groups, wrapped around the molecule. The most common regions are colored red and blue which implies a significant influence of classical and non-classical hydrogen interactions in the crystal packing of **2-Cl-Se**. The presence of ocher colored regions indicating the existence of aromatic interactions, which are the smallest part of FIM. Fig. 5B shows a hotspots which represent the positions of highest local density for each contour surface colored with the same colors as the corresponding part of the 3D surface. Arrangement of donor and acceptor functional groups is in good correlation with

the surface area included in intermolecular interactions obtained by Hirshfeld surface analysis.

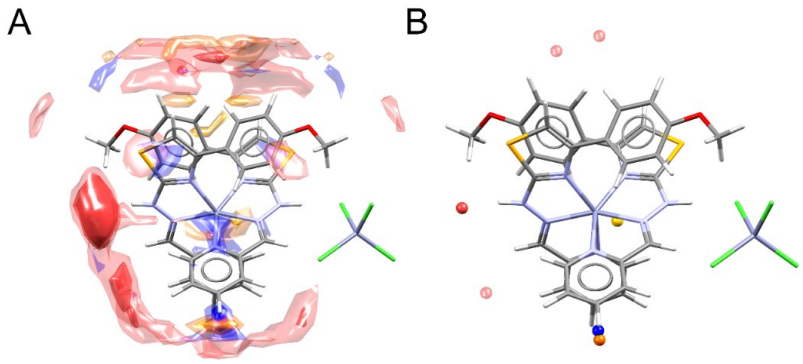

Fig. 5. Contour surface colored red (hydrogen bond acceptors), blue (hydrogen bond donors) and ocher (interactions which includes aromatic part of molecules) (A); the positions of highest local density for each contour surface showed as hotspots (B) around **2-Cl-Se**.

Energy distribution of intermolecular interactions

The use of B3LYP functional[43-46] and DGDZVP basis set[47,48] in investigations of molecular crystals based on metal coordination compounds, organic salts and solvates, as well as open shell molecules (radicals), provide a sufficiently good relative ratio of computing time and quality of obtained results.[49] The energy models in CrystalExplorer21[41] are calibrated and include optimum scale factors for B3LYP functional[49] (Table II). In the crystal structures of isosteres, there is the same trend in energy values. The nature of stabilizing interactions is predominantly electrostatic, with a significantly smaller contribution of polarization and dispersion components (Table II). Interactions in crystal structure of **2-Cl**[4] (Table S-III, Supplementary material) are realized at shorter distances (0.1–0.3 Å), thus attractive interactions are stronger (1–6 kJ mol^{-1}) than those in **2-Cl-Se**. The repulsive interactions are also more pronounced in **2-Cl**, while the polarization and dispersion components differ in the interval of 1–3 kJ mol^{-1}. The crystal packing energy represented as the sum of *E*_tot values is –1330.7 and –1322.0 kJ mol^{-1} for **2-Cl-Se** and **2-Cl**, respectively, thus the crystal packing energy of selenium based isostere is more stable by –8.7 kJ mol^{-1}. This difference comes from isosteric replacement of the sulfur by the selenium atom and arises from the nature of the selenium atom.

In order to visualize intermolecular interaction energies, using the calculated interaction energies in Table II the energy framework was calculated (Fig. 6). Since **2-Cl-Se** and **2-Cl** crystallize in the same space group, topology of the energies that stabilize and destabilize the crystal packing is complex but the same

pattern is observed for both isosteres.[4] The strongest interactions are realized in 3D, but mostly along the *a*-crystallographic axis while the repulsive interactions are located along the *b* and *c*-crystallographic axes. The calculated pattern confirms three-dimensional crystal packing based on geometrical parameters (*vide supra*).

TABLE II. Interaction pair energies in the crystal structure of **2-Cl-Se** based on the B3LYP/ /DGDZVP energy model; *E*_tot represents the sum of individual components with scaling factors (*k*_ele = 1.057; *k*_pol = 0.740; *k*_dis = 0.871; *k*_rep = 0.618), while the individual components are not scaled

R / Å	Energy component				
	*E*_ele	*E*_pol	*E*_dis	*E*_rep	*E*_tot
7.39	547.4	–72.0	–119.2	114.5	492.4
11.80	550.9	–51.3	–15.9	3.4	532.7
11.79	480.4	–43.0	–30.7	19.9	461.6
8.37	–622.6	–76.0	–11.7	17.1	–714.1
9.90	–632.4	–65.8	–11.1	15.6	–717.3
14.43	407.1	–21.5	–11.3	0.0	404.7
7.53	–858.7	–162.3	–28.9	102.8	–989.6
7.18	–662.0	–130.4	–26.1	29.2	–801.1

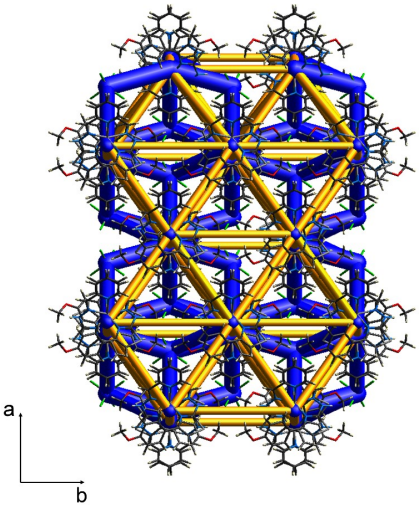

Fig. 6. Diagram of the energy framework of the total energies for the supercell (2×2×2) of the **2-Cl-Se**. The figure shows cylinders of the same scale (blue cylinders represent total energy, while yellow cylinders represent destabilizing energy).

CONCLUSION

The synthesis, structural characterization (spectroscopic and SCXRD), crystallographic and DFT analysis of crystal packing and intermolecular interactions of a new octahedral Zn(II) complex with a ligand from the pyridine-based 1,3--selenazolyl hydrazone class was performed. The two ligands are coordinated in

the neutral form by chelate *NNN*-tridentate forming a complex cation, while the anion is $[ZnCl_4]^{2-}$. The results of a comparative crystallographic study showed that novel complex crystallize in the same space group and has the same topology of intermolecular interactions as its sulfur isostere. However, due to nature of selenium, the crystal packing energy of Se-based isostere is higher by –8.7 kJ mol^{-1}. Hirshfeld surface analysis showed that the interactions involving the Se atom are more prevalent than the analogous ones in the S-based isostere which confirms additional contribution of the Se atom to the stabilization of the crystal packing.

SUPPLEMENTARY MATERIAL

Additional data and information are available electronically at the pages of journal website: https://www.shd-pub.org.rs/index.php/JSCS/article/view/12573, or from the corresponding author on request. CCDC 2269543-2269546.

Acknowledgement. The authors gratefully acknowledge financial support from the Ministry of Science, Technological Development and Innovation of Republic of Serbia, contract numbers 451-03-47/2023-01/200168, 451-03-47/2023-01/200288 and 451-03-47/2023-01/ /200116.

И З В О Д

Zn(II) КОМПЛЕКС СА 1,3-СЕЛЕНАЗОЛИЛ-ХИДРАЗОНОМ НА БАЗИ ПИРИДИНА: СИНТЕЗА, СТРУКТУРНА КАРАКТЕРИЗАЦИЈА И DFT СТУДИЈА

ЈОВАНА Б. АРАШКОВ[1], ПРЕДРАГ Г. РИСТИЋ[1], ALEKSANDAR VIŠNJEVAC[2], АНДРЕЈ Љ. МИЛИВОЈАЦ[3], ДРАГАНА М. МИТИЋ[3], НЕНАД Р. ФИЛИПОВИЋ[4] и ТАМАРА Р. ТОДОРОВИЋ[1]

[1]Универзитет у Београду – Хемијски факултет, Студентски трг 12–16, 11000 Београд, [2]Division of Physical Chemistry, Institute Ruđer Bošković, Bijenička cesta 54, Zagreb 10000, Croatia, [3]Иновациони центар Хемијског факултета, Универзитет у Београду, Студентски трг 12–16, 11000 Београд и [4]Универзитет у Београду – Пољопривредни факултет, Немањина 6, 11000 Београд

Октаедарски комплекс Zn(II) са лигандом из класе 1,3-селеназолил-хидразона на бази пиридина је синтетисан и окарактерисан IC и NMR спектроскопијом и дифракцијом X-зрака са монокристала. Чистоћа комплекса је потврђена елементалном анализом. Два лиганда су координована у неутралном NNN-тридентатном облику формирајући комплексни катјон, док је позитивно наелектрисање неутрализано помоћу $[ZnCl_4]^{2-}$. Комплекс кристалише у моноклиничној C2/*c* просторној групи при чему се атоми Zn(II) налазе у специјалном положају. Карактеристике кристалног паковања новог комплекса су анализиране употребом Хиршфелдових површина, конструкцијом 2Д псеудосиметричних графикона и употребом DFT квантномеханичких прорачуна при чему су добијени резултати упоређени са резултатима анализе претходно објављеног изоструктурног комплекса на бази сумпора. Идентификоване су кључне разлике у структурама које произилазе из изостерне замене атома сумпора атомом селена.

(Примљено 31. августа, ревидирано 25. септембра, прихваћено 13. октобра 2023)

REFERENCES

1. Y. Su, I. Cockerill, Y. Wang, Y. X. Qin, L. Chang, Y. Zheng, D. Zhu, *Trends Biotechnol.* **37** (2019) 428 (https://doi.org/10.1016/j.tibtech.2018.10.009)

2. T. Zhang, X. Li, Y. Qiu, P. Su, W. Xu, H. Zhong, H. Zhang, *J. Catal.* **357** (2018) 154 (https://doi.org/10.1016/j.jcat.2017.11.003)
3. D. Drozd, K. Szczubiałka, Ł. Łapok, M. Skiba, H. Patel, S. M. Gorun, M. Nowakowska, *Appl. Catal., B* **125** (2012) 35 (https://doi.org/10.1016/j.apcatb.2012.05.021)
4. J. B. Araškov, A. Višnjevac, J. Popović, V. Blagojević, H. S. Fernandes, S. F. Sousa, I. Novaković, J. M. Padrón, B. B. Holló, M. Monge, M. Rodríguez-Castillo, J. M. López--De-Luzuriaga, N. R. Filipović, T. R. Todorović, *CrystEngComm* **24** (2022) 5194 (https://doi.org/10.1039/d2ce00443g)
5. Z. Li, A. Dellali, J. Malik, M. Motevalli, R. M. Nix, T. Olukoya, Y. Peng, H. Ye, W. P. Gillin, I. Hernández, P. B. Wyatt, *Inorg. Chem.* **52** (2013) 1379 (https://doi.org/10.1021/ic302063u)
6. S. D. Han, N. N. Rajput, X. Qu, B. Pan, M. He, M. S. Ferrandon, C. Liao, K. A. Persson, A. K. Burrell, *ACS Appl. Mater. Interfaces* **8** (2016) 3021 (https://doi.org/10.1021/acsami.5b10024)
7. C. R. Groom, I. J. Bruno, M. P. Lightfoot, S. C. Ward, *Acta Crystallogr., B* **72** (2016) 171 (https://doi.org/10.1107/S2052520616003954)
8. P. Ristić, V. Blagojević, G. Janjić, M. Rodić, P. Vulić, M. Donnard, M. Gulea, A. Chylewska, M. Makowski, T. Todorović, N. Filipović, *Cryst. Growth Des.* **20** (2020) 3018 (https://doi.org/10.1021/acs.cgd.9b01661)
9. N. J. Williams, W. Gan, J. H. Reibenspies, R. D. Hancock, *Inorg. Chem.* **48** (2009) 1407 (https://doi.org/10.1021/ic801403s)
10. Z. Xun-Zhong, F. An-Sheng, Z. Fu-Ran, L. Min-Cheng, L. Yan-Zhi, M. Meng, L. Yu, *Bioinorg. Chem. Appl.* **2020** (2020) 1 (https://doi.org/10.1155/2020/8852470)
11. X. Zou, Y. Liao, C. Yang, A. Feng, X. Xu, H. Jiang, Y. Li, *J. Coord. Chem.* **74** (2021) 1009 (https://doi.org/10.1080/00958972.2020.1869952)
12. J. B. Araškov, M. Nikolić, S. Armaković, S. Armaković, M. Rodić, A. Višnjevac, J. M. Padrón, T. R. Todorović, N. R. Filipović, *J. Mol. Struct.* **1240** (2021) 130512 (https://doi.org/10.1016/j.molstruc.2021.130512)
13. L. K. Durgeswari, R. K. Ganta, Y. L. N. Murthy, *Russ. J. Org. Chem.* **57** (2021) 1552 (https://doi.org/10.1134/s1070428021090232)
14. A. A. Alfi, A. Alharbi, J. Qurban, M. M. Abualnaja, H. M. Abumelha, F. A. Saad, N. M. El-Metwaly, *J. Mol. Struct.* **1267** (2022) 133582 (https://doi.org/10.1016/j.molstruc.2022.133582)
15. V. A. Adole, R. A. More, B. S. Jagdale, T. B. Pawar, S. S. Chobe, *ChemistrySelect* **5** (2020) 2778 (https://doi.org/10.1002/slct.201904609)
16. S. Abu-Melha, *Pigment Resin Technol.* **48** (2019) 375 (https://doi.org/10.1108/PRT-09-2018-0102)
17. G. S. Masaret, *ChemistrySelect* **6** (2021) 974 (https://doi.org/10.1002/slct.202004304)
18. M. S. Shah, M. M. Rahman, M. D. Islam, A. Al-Macktuf, J. U. Ahmed, H. Nishino, M. A. Haque, *J. Mol. Struct.* **1248** (2022) 131465 (https://doi.org/10.1016/j.molstruc.2021.131465)
19. O. A. El-Khouly, M. A. Henen, M. A. A. El-Sayed, M. I. Shabaan, S. M. El-Messery, *Bioorganic Med. Chem.* **31** (2021) 115976 (https://doi.org/10.1016/j.bmc.2020.115976)
20. R. M. Kassab, S. M. Gomha, S. A. Al-Hussain, A. S. Abo Dena, M. M. Abdel-Aziz, M. E. A. Zaki, Z. A. Muhammad, *Arab. J. Chem.* **14** (2021) 103396 (https://doi.org/10.1016/j.arabjc.2021.103396)
21. S. Abu-Melha, *Arab. J. Chem.* **15** (2022) 103898 (https://doi.org/10.1016/j.arabjc.2022.103898)

22. A. Y. Alzahrani, Y. A. Ammar, M. Abu-Elghait, M. A. Salem, M. A. Assiri, T. E. Ali, A. Ragab, *Bioorg. Chem.* **119** (2022) 105571 (https://doi.org/10.1016/j.bioorg.2021.105571)
23. A. Pricopie, I. Ionuţ, G. Marc, A. Arseniu, L. Vlase, A. Grozav, L. Găină, D. C. Vodnar, A. Pîrnău, B. Tiperciuc, O. Oniga, *Molecules* **24** (2019) 3435 (https://doi.org/10.3390/molecules24193435)
24. N. J. C. Oliveira, I. N. S. Teixeira, P. O. Fernandes, G. C. Veríssimo, A. D. Valério, C. P. de S. Moreira, T. R. Freitas, A. C. V. Fonseca, A. de P. Sabino, S. Johann, V. G. Maltarollo, R. B. de Oliveira, *J. Mol. Struct.* **1267** (2022) (https://doi.org/10.1016/j.molstruc.2022.133573)
25. R. Gondru, S. Kanugala, S. Raj, C. Ganesh Kumar, M. Pasupuleti, J. Banothu, R. Bavantula, *Bioorganic Med. Chem. Lett.* **33** (2021) 127746 (https://doi.org/10.1016/j.bmcl.2020.127746)
26. S. Mor, S. Sindhu, S. Nagoria, M. Khatri, P. Garg, H. Sandhu, A. Kumar, *J. Heterocycl. Chem.* **56** (2019) 1622 (https://doi.org/10.1002/jhet.3548)
27. M. R. Shaaban, T. A. Farghaly, A. M. R. Alsaedi, *Polycycl. Aromat. Compd.* **42** (2022) 2521 (https://doi.org/10.1080/10406638.2020.1837887)
28. A. Pricopie, M. Focşan, I. Ionuţ, G. Marc, L. Vlase, L. Găină, D. C. Vodnar, E. Simon, G. Barta, A. Pîrnău, O. Oniga, *Molecules* **25** (2020) 1079 (https://doi.org/10.3390/molecules25051079)
29. S. S. Jadav, V. N. Badavath, R. Ganesan, N. M. Ganta, D. Besson, V. Jayaprakash, *Anti--Infective Agents* **18** (2018) 101 (https://doi.org/10.2174/2211352516666181016122537)
30. M. V. de O. Cardoso, G. B. de Oliveira Filho, L. R. P. de Siqueira, J. W. P. Espíndola, E. B. da Silva, A. P. de O. Mendes, V. R. A. Pereira, M. C. A. B. de Castro, R. S. Ferreira, F. S. Villela, F. M. R. da Costa, C. S. Meira, D. R. M. Moreira, M. B. P. Soares, A. C. L. Leite, *Eur. J. Med. Chem.* **180** (2019) 191 (https://doi.org/10.1016/j.ejmech.2019.07.018)
31. A. Višnjevac, J. B. Araškov, M. Nikolić, Ž. Bojić-Trbojević, A. Pirković, D. Dekanski, D. Mitić, V. Blagojević, N. R. Filipović, T. R. Todorović, *J. Mol. Struct.* **1281** (2023) 135193 (https://doi.org/10.1016/j.molstruc.2023.135193)
32. D. Radomska, R. Czarnomysy, D. Radomski, A. Bielawska, K. Bielawski, *Nutrients* **13** (2021) 1 (https://doi.org/10.3390/nu13051649)
33. D. Radomska, R. Czarnomysy, D. Radomski, K. Bielawski, *Int. J. Mol. Sci.* **22** (2021) 1 (https://doi.org/10.3390/ijms22031009)
34. N. R. Filipović, H. Elshaflu, S. Grubišić, L. S. Jovanović, M. Rodić, I. Novaković, A. Malešević, I. S. Djordjević, H. Li, N. Šojić, A. Marinković, T. R. Todorović, *Dalt. Trans.* **46** (2017) 2910 (https://doi.org/10.1039/c6dt04785h)
35. Agilent Technologies UK Ltd., *CrysAlisPro Software system*, 2014 (n.d.)
36. G. M. Sheldrick, *Acta Crystallogr., C* **71** (2015) 3 (https://doi.org/10.1107/S2053229614024218)
37. A. L. Spek, *Acta Crystallogr., D* **65** (2009) 148 (https://doi.org/10.1107/S090744490804362X)
38. C. F. MacRae, I. Sovago, S. J. Cottrell, P. T. A. Galek, P. McCabe, E. Pidcock, M. Platings, G. P. Shields, J. S. Stevens, M. Towler, P. A. Wood, *J. Appl. Crystallogr.* **53** (2020) 226 (https://doi.org/10.1107/S1600576719014092)
39. L. J. Farrugia, *J. Appl. Crystallogr.* **45** (2012) 849 (https://doi.org/10.1107/S0021889812029111)
40. O. V. Dolomanov, L. J. Bourhis, R. J. Gildea, J. A. K. Howard, H. Puschmann, *J. Appl. Crystallogr.* **42** (2009) 339 (https://doi.org/10.1107/S0021889808042726)

41. P. R. Spackman, M. J. Turner, J. J. McKinnon, S. K. Wolff, D. J. Grimwood, D. Jayatilaka, M. A. Spackman, *J. Appl. Crystallogr.* **54** (2021) 1006 (https://doi.org/10.1107/S1600576721002910)
42. *Gaussian 09, Revision A.02*, Gaussian, Inc., Wallingford, CT, 2009
43. T. Lecklider, *EE Eval. Eng.* **50** (2011) 36 (https://go.gale.com/ps/i.do?p=AONE&u=anon~9e9d6b50&id=GALE|A272486022&v=2.1&it=r&sid=googleScholar&asid=467f45d4)
44. A. D. Becke, *J. Chem. Phys.* **104** (1996) 1040 (https://doi.org/10.1063/1.470829)
45. A. D. Becke, *J. Chem. Phys.* **96** (1992) 2155 (https://doi.org/10.1063/1.462066)
46. A. D. Becke, *J. Chem. Phys.* **98** (1993) 5648 (https://doi.org/10.1063/1.464913)
47. N. Godbout, D. R. Salahub, J. Andzelm, E. Wimmer, *Can. J. Chem*. **70** (1992) 560 (https://doi.org/10.1139/v92-079)
48. C. Sosa, J. Andzelm, B. C. Elkin, E. Wimmer, K. D. Dobbs, D. A. Dixon, *J. Phys. Chem*. **96** (1992) 6630 (https://doi.org/10.1021/j100195a022)
49. C. F. Mackenzie, P. R. Spackman, D. Jayatilaka, M. A. Spackman, *IUCrJ* **4** (2017) 575 (https://doi.org/10.1107/S205225251700848X).